Nuclear Instruments and Methods 206 (1983) 341–351
North-Holland Publishing Company

OASIS: THE SUPERHILAC ON-LINE ISOTOPE SEPARATOR *

J. Michael NITSCHKE
Nuclear Science Division, Lawrence Berkeley Laboratory, University of California, Berkeley, California 94720, U.S.A.

Received 1 September 1982

An on-line isotope separator at the Berkeley SuperHILAC is described. It is based on a gas-cooled target coupled with a surface ion source or with a newly developed space-charge compensated electron-bombardment source. Compound nucleus and damped reactions can be used for isotope production. The analyzing magnet is a 180° sector field with a field index of 0.5. Several operating features described include beam intensity measurements and computer control, and the detection systems. Some preliminary off-line and on-line results are reported.

1. Introduction

On-line isotope separators (ISOL) have been discussed extensively at recent conferences [1,2] and in review articles [3–5]. Besides its obvious contributions to almost all aspects of nuclear physics, on-line isotope separation has been applied to several other branches of physics, such as optics, solid-state, atomic, and particle physics, and even chemistry and medicine. The most famous member of the ISOL family is ISOLDE at CERN. With 1 μA of 600 MeV protons and target thicknesses of up to 150 g/cm^2, it provides isotope-separated radioactive beams of more than 10^{11} ions/s for the most abundant species [6]. At heavy ion accelerators, the production yield for isotopes near beta stability is about six orders of magnitude lower. The situation, however, is different for isotopes *far* from stability (at about mass 114 for Xe/Cs, for example), where heavy ion (HI) induced compound nucleus (CN) reactions are the only known means of producing nuclei near the proton drip line. This has been demonstrated recently at GSI with the synthesis of ^{151}Lu and ^{147}Tm [7], which provide the first evidence for proton decay from the ground state. Besides GSI, several other laboratories have proven that isotope separation on-line with a heavy ion accelerator is a viable concept.

At the heavy ion linear accelerator (HILAC) in Berkeley, the first on-line isotope separation was performed in 1968 utilizing a quadrupole mass spectrometer [8]. After the the accelerator was upgraded into the SuperHILAC in 1971, experiments were started to realize a long-sought goal: to thermalize highly charged recoils in a suitable gas (i.e., ultra-pure helium at about 1 atm pressure), have them recapture all their electrons except one, reacclerate the singly charged atoms to a fixed energy of several keV, and analyze them in a conventional magnetic spectrometer. This concept worked successfully in *off*-line experiments with α-recoil sources like ^{227}Ac and ^{228}Th, where oveall efficiencies of several percent were obtained and the members of the α-decay series separated easily. In the presence of the intense accelerator beam, however, a high-density plasma was created through the interaction of the beam with the stopping gas, and most of the thermalized, singly charged recoils become neutralized. In addition, atomic reactions cotribute to the neutralization of the recoils in on-line experiments. These reactions are caused by impurity ions, like H_2O^+, liberated from the wall of the target chamber and the target itself. The two dominating neutralizing reactions for a recoil ion R^+ are: $R^+ + e^- + He \rightarrow R + He$, and $R^+ + e^- + e^- \rightarrow R + e^-$.

Since the three-body recombiation coefficients for these reations depend strongly on the electron temperature (proportional to $T_e^{-2.5}$ and $T_e^{-4.2}$, respectively), two methods of heating the plasma were investigated: radio-frequency (rf) heating and a dc discharge. To obtain a short delay time inside the ion source, the stopping chamber must be small. This makes rf heating impractical because rf power cannot be concentrated very easily in a small volume (except by using microwaves). Heating with a dc arc, however, is quite localized. The highest plasma temperature achieved so far with arc heating is about 6800 K, and, at this temperature thermal ionization becomes significant. This process is governed by the Saha equation:

$$\eta \propto \frac{1}{P_e} T^{5/2} \frac{Z_i}{Z_a} 10^{-[(5040/T)V_{eff}]}.$$

* This work was supported by the Director, Office of Energy Research, Office of High Energy and Nuclear Physics, Nuclear Science Division, U.S. Department of Energy under Contract No. DE-AC03-76SF00098.

0167-5087/83/0000–0000/$03.00

Here, $\eta = n_i/n_a$ is the degree of ionization, P_e the electron pressure, Z_i and Z_a the ion/atom partition functions, T the equilibrium temperature, and V_{eff} the effective ionization potential.

This investigation led to the development of a new method to ionize trace impurities in the presence of a much larger amount of carrier gas. With a typical electron pressure of 3×10^{-4} atm and a plasma temperature of 6800 K, ionization efficiencies of greater than 10% can be achieved for elements with ionization potentials $V_{eff} \leq 10$ eV. This includes 85% of all elements of the periodic table. The carrier gas helium, on the other hand, having a first ionization potential of 24.5 eV, is ionized with an efficiency of only 1.2×10^{-11} (6800 K). Therefore, at a He gas (neutral) flow of 10 Torr $\cdot$ l $\cdot$ s^{-1}, the He^+ current is only 5×10^{-10} A, much less than the currents of impurity ions, which are on the order of 10^{-6} A. Thus far, the following elements have been ionized with this carrier-gas method: (He), Ar, Kr, Xe, Rn, Ag, W, Hg, and Th. The experimentally determined ionization efficiencies agree with the Saha equation if an effective plasma temperature of 6500 K and an electron pressure of 3×10^{-4} atm are assumed.

This new type of ion source is still under development. Two other types – a surface ionization source and a space-charge compensated electron bombardment source (SC-EBIS) – are now in routine operation and will be described later.

2. General layout

Fig. 1 shows the experimental area of the SuperHILAC and the location of the **O**n-line **A**pparatus for **S**uperHILAC **I**sotope **S**eparation (OASIS) in the north cave area (cave N). The general layout of the separator will in the following be discussed with reference to fig. 2. The E89 beam line leading to the separator includes, besides the usual optical components and diagnostic tools, a "wobbler" to make the beam spot on the target move in a circular path. This leads to a uniform temperature distribution over the surface of the target and allows for high beam intensities. The wobbler consists of an ordinary three-phase motor, with the rotor replaced by the beam pipe. The stator coils are energized by an 800 Hz three-phase current, which is matched to the target diameter to obtain an optimal temperature distribution.

Before the beam impinges on the target, it traverses a RF pickup electrode that measures the beam intensity. The target/ion source arrangement (fig. 2) is one of several possible combinations, as will be discussed later. In the case shown, the target is gas cooled [9,10]. It is followed by heat shields and absorbers to reduce the energy of the target recoils if necessary. The recoils then enter the ion source, where they are stopped in a suitable catcher material (typically Ta). All OASIS ion sources are operated at high temperatures, in some cases

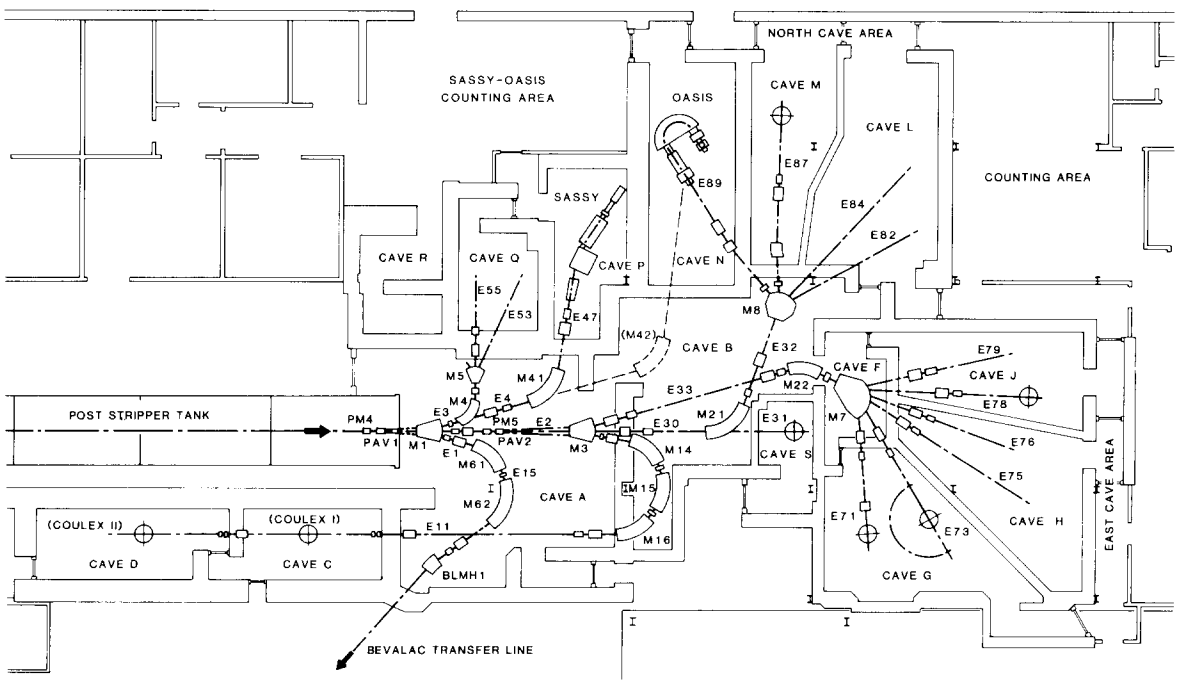

Fig. 1. General layout of the SuperHILAC target showing the location of the on-line isotope separator (OASIS) in cave N (top center).

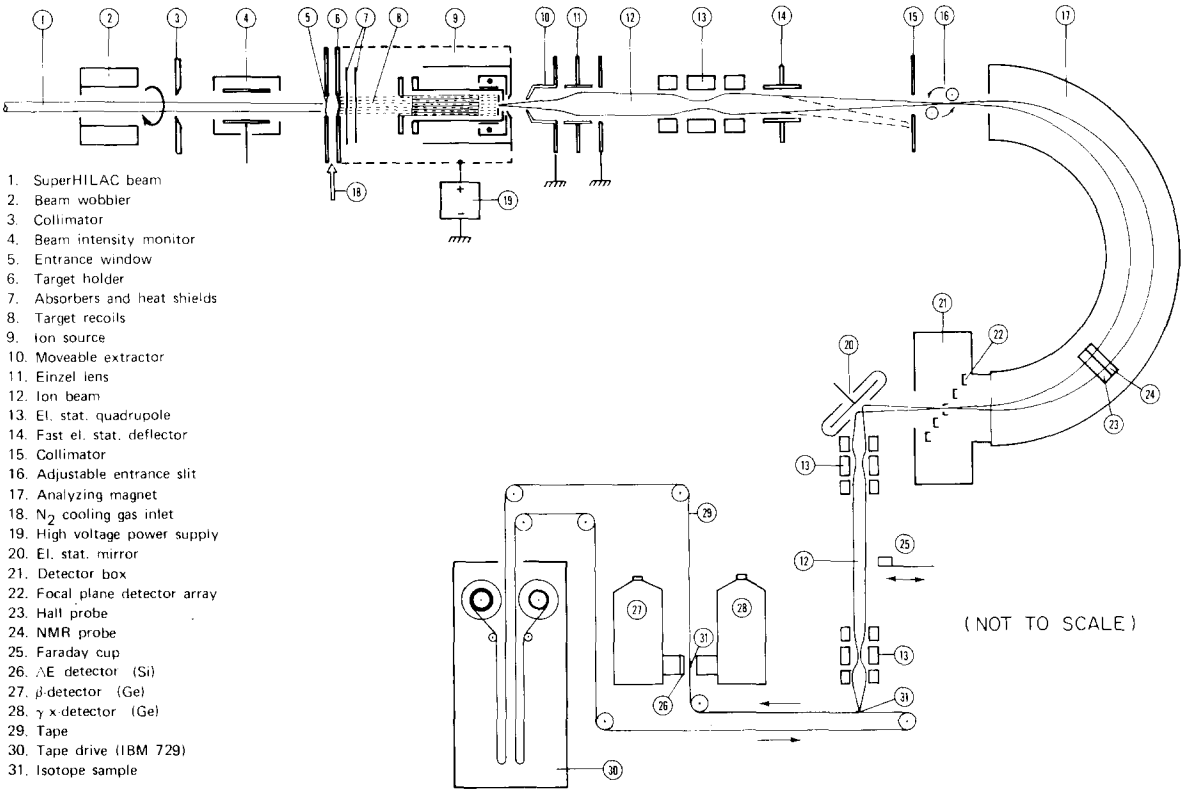

Fig. 2. Schematic representation of OASIS showing its main components. The electrostatic mirror (20) deflects the beam vertically (shown turned 90°) to the next floor of the laboratory.

close to the melting point of Ta (~ 3000°C). This allows for a fast diffusion of the recoils out of the stopping material and a short delay time inside the source. After ionization, the recoils are extracted axially and accelerated to 50 keV in a single step. The extraction electrode can be biased negatively with respect to ground for space-charge neutralization; its distance from the ion source is variable by remote control.

A few centimeters behind the extraction electrode is an einzel lens that can be operated between 0 and 50 kV. It is followed by an electrostatic quadrupole triplet that focuses the beam onto the entrance slit of the actual magnetic spectrometer. Details of the magnet design will be covered in the next section. Depending on the kind of nuclear spectroscopy to be carried out, the mass-dispersed ion beams can be stopped directly behind the spectrometer magnet in a detector chamber, or a single selected isotope can be transported via an electrostatic mirror and two quadrupole triplets to a shielded room 4 m above the separator. This is necessary because the beam from the SuperHILAC is stopped in the ion source, which is only 1.5 m from the detector chamber. This proximity causes a large β-, γ-, and n-background, and makes the spectroscopy of other than charged particles (i.e., p, α, and SF) difficult or impossible. The identification of neutron-rich light β-emitters inside the "cave" has, however, been achieved with a Si ΔE–E β-telescope operated at 80 K. High resolution, low-background β–γ spectroscopy will be carried out after the completion of the tape system at the end of the isotope transport line.

3. Construction details

3.1. Ion optical considerations

The ion optical properties of the on-line separator have been optimized by using a first-order interactive computer program based on a matrix theory [11]. Fig. 3 represents the results of one of these calculations; only the major components are shown, although the calculation was carried out with the complete set of matrices, including those for extraction and acceleration of the ions. The solid lines indicate the evolution of the beam envelope in the x- (radial) plane and the y- (axial) plane for a beam of 50 cm · mrad initial emittance at the ion source (i.e., *before* acceleration). The four dashed lines indicate positive and negative x- and y-vectors of a test particle.

The electrostatic quadrupole triplets Q_1, Q_2, and Q_3 provide ion optical flexibility by being able to change

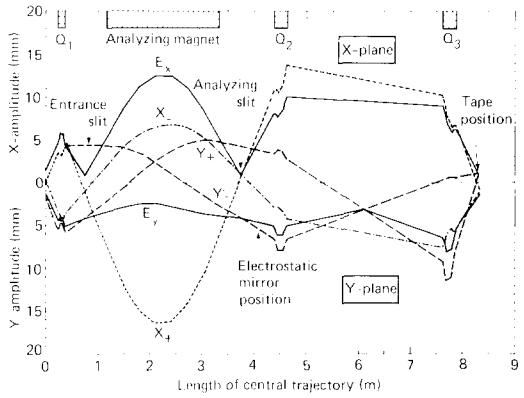

Fig. 3. Results of first order calculations of the OASIS ion optics. The x-plane is horizontal, the y-plane vertical. Q_1 through Q_3 are electrostatic quadrupole triplets. The curves labled E_x and E_y represent the beam envelopes in the horizontal and vertical plane. The source emittance is assumed to be 500 mm mrad. $X_\pm$ and $Y_\pm$ are vectors of a test particle (mass: 250 amu) with initial values of ± 1 mm and ± 500 mrad for position and divergence, respectively.

the beam envelope in all parts of the separator. Adjusting Q_1, for instance, makes it possible to obtain a point-to-point, point-to-slit, or slit-to-slit relationship between object and image at the entrance and exit of the magnet. The latter case is shown in fig. 3: In the radial (X) plane, beam cross-overs are created at the position of the object and image slit, while the beam in the axial (y) plane is relatively wide at these positions. To obtain a large axial acceptance, a y-crossover is generated after the beam has made a 90° turn in the magnet. A similar principle is applied to the transfer line where Q_2 produces a nearly parallel beam in the x-plane and a crossover in the y-plane, which again minimizes the size of the beam envelope. The function of Q_3 is to focus the selected isotope on a detector or tape. The distance between Q_3 and the focal point determines the overall (ion source-to-detector) magnification, which is -0.72 in the x-plane and -1.09 in the y-plane. As indicated in fig. 3, the electrostatic mirror is positioned close to the analyzing slit to keep its size to a minimum. It is operated at about 80% of the accelerating potential. In addition, electrodes are located behind each of the three quadrupoles to correct for small deviations of the beam from the ideal, central trajectory. The x-deflection electrodes following Q_1 are in addition connected to a fast, switchable power supply which can be triggered from several sources, interrupting the beam within 10 μs. This feature is useful for half-life measurements, for instance. It also prevents isotopic cross-contamination in case of a high-voltage breakdown due to sparks. Finally, the einzel lens that forms an integral part of the movable extraction electrode (fig. 2) matches the beam emittance of experimental ion sources to the remaining components of the separator.

3.2. The magnet

The main analyzing magnet of the OASIS facility was *not* intended for on-line isotope separation but rather to analyze unslowed reaction products from targets bombarded with 10.3 MeV/A beams from the "old" HILAC. In its present use, it is operated at about one-half of its design field, so saturation effects are minimal. For an ion of mass 300 and an energy of 50 keV, the mean field is only 0.8 T and Br_0 is 0.53 Tm. The basic parameters of the magnet are: sector angle $\theta = 180°$, mean radius of curvature $r_0 = 0.66$ m, and first field index $\alpha = 0.5$ (for the definition of α, see below). The focusing properties, aberrations, and fringing effects of this type of spectrometer have been discussed in refs. 12 and 13, where it is shown that the momentum (P) dispersion D_P is given by the simple formula $D_P = (1 + M_r)/(1 - \alpha)$, where M_r is the radial magnification, and D_P is defined as $D_P \equiv \Delta x/(\Delta P/P)$, with Δx and D_P measured in units of r_0. In the case of OASIS, the magnet is operated in the symmetric mode, which results in $M_r = 1$ and $D_p = 4$. From this the momentum resolution (R_p) can be determined if the object slit width (W) is known: $R_p = D_p/M_r W$. Assuming $W = 1.5$ mm, it follows that $R_p = 1761$, and, since the mass energy dispersion $D_m = 1/2 D_p$, the mass resolution R_m is about 880. This is adequate for the purpose of the instrument. The focal plane angle can be calculated from formulae given in ref. 13 and is, in this case, 29°, measured with respect to the central beam axis. The radial field distribution $B(r)$ in the magnet is described by

$$B(r) = B_0\left[1 - \alpha\left(\frac{r - r_0}{r_0}\right) + \beta\left(\frac{r - r_0}{r_0}\right)^2 + \gamma\left(\frac{r - r_0}{r_o}\right)^3 + \cdots\right].$$

For the OASIS magnet, $\alpha = 0.5$ was chosen to obtain equal object and image distances in the radial and the axial direction, and $\beta = 0.21$ ($\sim \alpha^2$) was eavluated from expressions given in ref. 13. It was found that even for the extreme case of $(r - r_0) = 75$ mm, neglecting the third order-term in the above equation contributes an error of only 0.02%, and γ was therefore set to zero. No corrective coils on the pole faces [14] are used even though slight adjustment in β could perhaps improve the mass resolution. "α-coils" are not necessary since the electrostatic quadrupole triplet Q_1 (fig. 2) can shift the beam crossovers over a wide range along the beam axis (see next section). Installating corrective coils would also be difficult because the magnet pole pieces constitute the top and bottom of the vacuum chamber. Table 1 summarizes the values of the main parameters of the separator magnet. It should be noted that the mass dispersion $D_m = 1.18$ m is smaller than calculated

Table 1
Principal parameters of the separator magnet.

Parameter	Definition	Value
Sector angle	θ	180°
Effective magnetic sector angle	θ'	186°
Mean radius	r_0	0.66 m
Field indices	α, β, γ	0.5, 0.21, 0
Focal plane angle	ϕ	29°
Magnifications (radial, axial)	m_r, m_a	1.0, 1.0
Image/object distance from effective field boundary	d	0.42 m
Area of aperture	A	$\geq 8.7 \times 10^{-3}$ m^2
Solid angle	$\Omega = A/(d^2 + 2r_0^2)$	≥ 8.4 msr
Mass dispersion	$D_M = \Delta x/(\Delta m/m)$	1.18 m
Mass resolving power (for 1.5 mm object slit)	$R_m = m/\Delta m$ (fwhm)	880
Mass range	$(M_{min} - M_{max})M_{min}$	15%
Separable masses (at 50 kV acceleration)	–	1 to 400 amu
Transmission	η	~ 95%
Weight	–	8900 kg

from the theoretical value of $D_p = 4$, which would give $D_m = 1/2r_0D_p = 1.32$ m. This is mostly due to two 16° wide, wedge-shaped pole pieces located at the 135° position of the 180° magnet. These pole pieces create a section of field sufficiently homogeneous to operate a nuclear magnetic resonance (NMR) probe for mass measurements, as will be described in section 4.

3.3. Beam intensity measurement

The determination of the intensity of the accelerator beam that impinges on the target is, in general, a straightforward problem. The conventional methods are to design the target as a Faraday cup that also stops the beam, or to let the beam traverse the target and catch it in a separate cup. In the case of an on-line isotope separator, however, neither method is feasible because the beam stops in a target–ion source combination that is operated at a high voltage potential of several tens of kilovolts. Therefore, the beam measuring system shown in fig. 4 was developed. It relies on the voltage induced by individual miroscopic beam bunches as they traverse an electrostatic pickup electrode. A microscopic beam bunch at the SuperHILAC is typically 1 to 3 cm long and has a repetition frequency of 70.289 MHz. As it passes through the 5 cm long pickup electrode, it induces a voltage (U) that is proportional to the charge (Q) carried by by the bunch, and inversely proportional to the capacity (C) of the electrode, i.e., $U = Q/C$. This signal has a fundamental frequency of 70.289 MHz and several harmonics, depending upon the degree of bunching or debunching of the beam. It is amplified in a preamplifier with 20 dB gain and 5 MHz bandwidth, and mixed down to an intermediate frequency (IF) of 1 MHz. The IF amplifier has a bandwidth of about 100 kHz and a gain of 80 dB; it is followed by a detection circuit, a gated integrator, and a sample-and-hold circuit. The momentary output of the sample-and-hold circuit is proportional to the integrated beam intensity during one macropulse. The shape of the macropulse is displayed at the output of the detection circuit. An

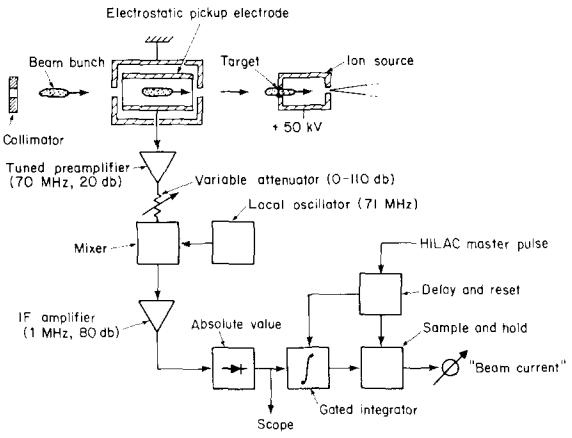

Fig. 4. Beam intensity measuring device. The collimator and the electrostatic pick-up electrode are located in front of the target/ion source on ground potential (see also fig. 2).

attenuator between the preamplifier and the mixer serves as a range switch. This device has been used in all on-line runs, and is generally calibrated by comparing its output to a conventional Faraday cup in order to avoid errors due to the varying microstructure of the beam.

3.4. Vacuum system

The vacuum system for OASIS was designed for a residual gas pressure on the order of 10^{-6} Torr to avoid excessive degradation of the beam due to scattering by neutral gas molecules. The ion source region is pumped by a baffled 250 mm (7000 l/s) diffusion pump. This high pumping speed is convenient when experimental ion sources with high gas throughput are tested. A second baffled diffusion pump (250 mm, 500 l/s) is located at the entrance of the magnet and is intended to differentially pump the remaining gas from the ion source. The analyzing magnet has a port at the 90° position, which is connected to a small (150 l/s) turbo pump. Vacuum in the detector chamber surrounding the focal plane is created by a cryopump with a speed of 1500 l/s for air and 4000 l/s for water. This assures a hydrocarbon "free" environment ($\sim 10^{-7}$ Torr) for the solid-state detectors and channeltrons frequently used in this area. The 4 m long transfer line from the cave to the counting room is pumped by two turbomulecular pumps (270 and 500 l/s).

Pressure measurements in various parts of OASIS are made with ion gauges. These gauges are operated by a control unit that provides an output signal proportional to the *logarithm* of the pressure and independent of the emission current. A range of 10^{-3} to 10^{-8} Torr is covered *without range switching*. This is advantageous for computer monitoring since the computer can easily calculate the "antilog" function to provide a conventional pressure indication.

3.5. Tape transport and detector system

As pointed out in section 3.2, the focal plane of the analyzing magnet is – for historical reasons – located inside the cave. The line-of-sight distance to the target/ion source is only about 1.5 m, and the angle to the accelerator beam axis is approximately 60°. Since the beam is stopped in the ion source, it causes a large background of neutron- and γ-radiation at the focal plane position which, in general, prevents the detection of similar radiation from separted isotopes. It is possible, however, to obtain spectroscopic information from SF-, p-, α-, and β-decay. For the β-spectroscopy of neutron-rich isotopes of light elements produced in damped collisions, a β-telescope has been built. It consists of a thin (150 μm Si) ΔE- and a thick (10 mm Si) E-detector, both operated at a temperature of about 80 K. Similarly, for the proton spectroscopy of selected isotopes, a dual ΔE-, E-Si-telescope is used; it is operated at room temperature.

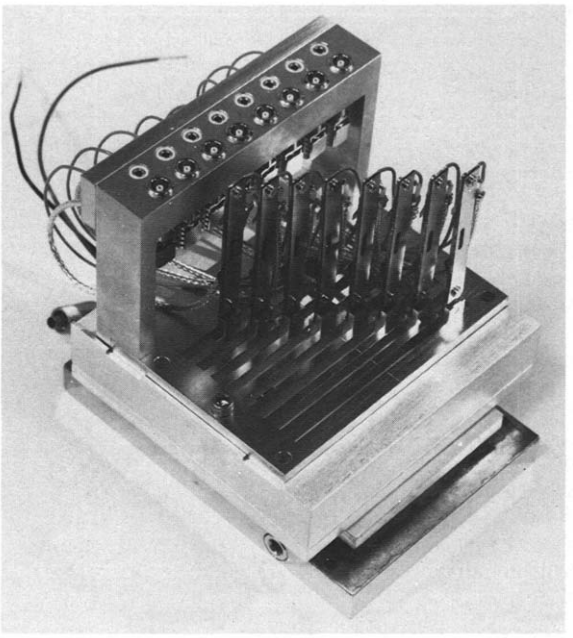

Fig. 5. Focal plane detector array consisting of 8 individual surface barrier detectors for the simultaneous study of 8 different isotopes. The detectors are mounted on a Peltier module that permits cooling to −40°C.

With the detector array shown in fig. 5, the α- and spontaneous fission decay of eight different isotopes can be studied simultaneously. The position of each detector can be adjusted to select the desired mass number and to allow for varying mass dispersion.

In the detector configurations described above, the 50 keV ion beams are stopped in 20 μg/cm² carbon foils located 1 or 2 mm in front of the respective detector surface. These foils are isolated from ground and located behind a collimator so that the beam current of individual isotopes can be optimized and monitored. Half-life measurements are generally carried out by deflecting the beam as described in section 3.1 and observing radioactive growth and decay.

A different focal plane detector system is based on a rotating drum periodically turned by a stepping motor. The axis of the drum lies in the central plane of the magnet and is perpendicular to the central ray at the exit. Several isotopes are deposited along a generatrix of the drum and are analyzed by peripheral detectors. Half-life information can be obtained from the rotation period of the drum and the position of the detectors.

In some cases, 47 mm long position-sensitive surface barrier detectors are used in the focal plane position. They are quite expensive, however, and have inferior

resolution compared to separate detectors for each isotope.

To carry out proton, γ-ray, X-ray, and neutron spectroscopy, the beam of a selected isotope is guided through the transfer line to a shielded room above the separator (see fig. 2). The ion beam is stopped in an aluminized Mylar or standard computer tape, which transports the activity to a detector system operated in close geometry. The tape is advanced through two vacuum locks by a surplus IBM-729 tape drive at a speed of 2.858 m/s. The distance between the collection point and the center of the detectors is about 18 cm. This results in a transport time of about 60 ms, comparable to the shortest delay times in the ion source. The two detectors facing each side of the tape have the following characteristics: (1) n-type Ge-coax 1.8 keV resolution (^{60}Co), 25% efficiency, and (2) high-purity Ge, 36 mm diameter, 13 mm thick, with a 50 μm thick Be window. Between detector (2) and the tape, a ΔE silicon-surface barrier detector (SSB) can be inserted. Detector (1) is primarily intended for the detection of photons between 10 keV and 10 MeV, while detector (2) is optimized for X-rays between 3 and 200 keV and, in conjunction with the SSB-ΔE detector, for β-particles up to 10 MeV *. If necessary, other charged particle detectors can be added between the tape and the Ge detectors. With this versatile system, coincidences and single events associated with the following radioactive decay modes can be detected: p, α, β, SF, X-ray, and γ.

4. Mass determination

The precise determination of the atomic mass number of the isotope under investigation depends on the exact measurement of the ion energy and the magnetic field of the analyzing magnet. The ion energy is determined by the accelerating potential, which is measured with a precision voltage divider and a 6-1/2-digit digital voltmeter. The magnetic field is meaured with a nuclear magnetic resonance (NMR) probe. Like all NMR probes, it has to be retuned manually whenever the magnetic field is changed (except for small variations). This is quite inconvenient because the NMR is linked to a computer that calculates the mass from the frequency and the ion energy. A device built at LBL eliminates any tuning and affords a completely automatic mass determination. Fig. 6 shows its principal components. A Hall probe and the NMR probe are placed adjacent to each other inside the homogeneous magnetic field section of the analyzing magnet (see section 3.2). Tuning of the NMR probe is carried out by the coarse frequency control voltage. This voltage is

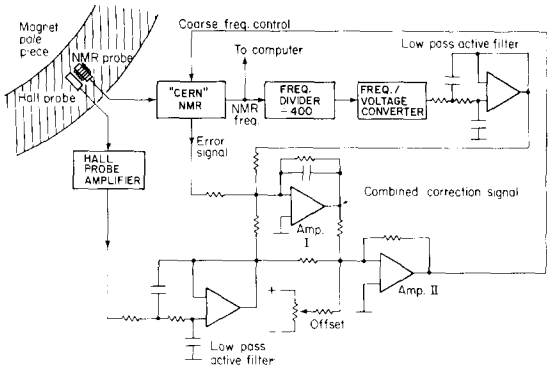

Fig. 6. Hall probe controlled nuclear magnetic resonance magnetometer. The magnetic field value together with the value of the accelerating potential are fed into the PDP 11/10 process control computer, which calculates the center mass of the separator (see also fig. 7).

derived from the Hall probe via the probe's amplifier, an active filter, and the summing amplifier Amp. II. An offset is introduced into Amp. II because the control voltage spans a range from 0 to 7 V, while the magnetic field varies from 3.5 to 10.5 kG. This primary control circuit would be sufficient for tuning the NMR if its frequency were a linear function of the control voltage. Since this is not the case, a correction signal is generated in Amp. I that compares the field measured by the Hall probe with the converted NMR frequency. In addition, an error signal from the NMR, and another offset voltage are added. This combined correction signal ensures perfect tracking between the field measured by the Hall probe and the NMR frequency control voltage, which amounts to an automatic tuning procedure. The function of the error signal is to lock the NMR signal to the zero crossing of the magnetic field modulation.

For an ion energy of 50 keV, the masses that can be determined automatically range from 45 to 380 amu, with a precision of ± 0.001 amu. Other mass ranges can be obtained by changing the NMR probe. For coarse tuning of the spectrometer, an additional mass meter is available. It is based on analog techniques using the hall probe signal (fig. 6) and the high voltage signal from the precision divider.

The process control computer (PDP 11/10) also monitors these two signals and performs a third mass calculation. The precision of the mass determinations based on the Hall probe measurements is only ± 0.1 to 0.01 amu over the range of 1 to 300 amu.

5. Computers

OASIS operates in conjunction with two computers: a PDP 11/10 for control and/or monitoring of almost all important instrumental parameters, and a Mod-

* A recent account of the use of high-purity Ge detectors for Q_β measurements is given in ref. 15.

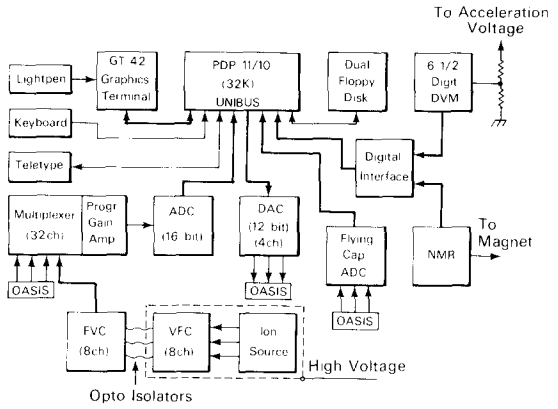

Fig. 7. OASIS computer control and monitor system. DVM: digital voltmeter; NMR: nuclear magnetic resonance probe; ADC: analog-to-digital converter; DAC: digital-to-analog converter; VFC: voltage-to-frequency converter; FVC: frequency-to-voltage converter. Heavy and fine lines indicate parallel and serial links, respectively.

Comp "Classic" for data taking and analysis. The ModComp "Classic" is part of a general purpose data acquisition facility at the SuperHILAC. It is basically an 800 ns, 16 bit computer with a maximum memory capacity of 1024 thousand words, linked to the detector electronics via a differential branch transceiver and CAMAC equipment. The software package called MINUS3 contains four independent tasks: "Chaos" inputs data from the ADC or event tapes; "Order" sorts data for display; "MultiD' displays and analyzes singles histograms; and "Space" displays two-dimensional histograms; for a detailed discussion, see ref. 16.

Fig. 7 shows a block diagram f the control computer and its peripheral devices. The PDP 11/10 is a small (32-thousand-word memory) 16-bit computer with a cycle time of 1 μs. Its RT-11 operating system supports the high-level language BASIC with a graphics extension. This combination allows for easy programming and quick changes in the display, monitoring, and control of different OASIS parameters. Assembly language subroutines are used to facilitate communication between the different interfaces and BASIC. The workhorse of the control system is the 32-channel multiplexer which has differential inputs, programmable gain (1, 10, 100, and 500), and a resolution of 16 bits. Its throughput rate is 2.5 kHz.

The monitoring of the ion source parameters on high voltage potential (50 kV) is achieved by a combination of voltage- (or current-) to-frequency converters (VFC), optical isolators, and frequency-to-voltage converters (FVC) on ground potential. Closed-loop feedback systems exist to stabilize the acceleration voltage, the magnet current and the ion source anode current.

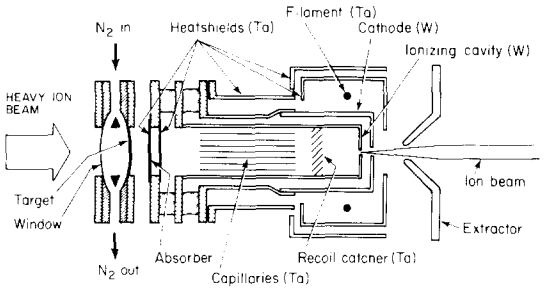

Fig. 8. Schematic diagram of the surface ion source with a gas-cooled target for the study of compound nucleus evaporation residues.

6. Ion sources and targets

The two most important qualities of an ion source suitable for on-line isotope separation are high efficiency and short delay time. These requirements are often coupled with additional demands for universality, long lifetime, stability, good beam quality, and chemical selectivity. Several of these conditions clearly are mutually exclusive and cannot be realized in a single type of source, particularly if one considers that the ion source sometimes has to be coupled to very fragile and/or radioactive targets. Ref. 17 reviews recent progress in ion source developments for on-line isotope separators.

Fig. 8 shows a schematic representation of one of the surface ionization sources used at OASIS. The target is in general of the type described in ref. 9 and consists of an entrance and exit window with the target material deposited on the latter. A stream of high-velocity nitrogen gas passes between the two window foils and removes the heat generated by the accelerator beam and the thermal radiation from the source. The target is followed by two heat shields (20–100 μg of carbon) which can also be used to degrade the energy of the recoils. This reduces the recoil range in the catcher and consequently the diffusion time to the catcher surface. For the production of isotopes via damped reactions, where the recoil products have wide angular distribution, the target is moved closer to the ionization region. Under these conditions, the target is operated near the temperature of the catcher, and the choice of target material is restricted to Ta, W, and ThO_2. In the case shown in fig. 8, the ionization of the recoils takes place on the hot ($> 2500°C$) walls of a tungsten cavity. This cavity is heated by electron bombardment from a coaxial cathode heated in turn by electron bombardment from a coaxial filament. The reason for this double electron bombardment is that the mantle of the tungsten cavity can be replaced by a grid that then converts the source to an electron bombardment type [18]. The target and the ion source are operated at a high voltage potential,

typically 50 kV. The extraction electrode is at ground potential and can be moved in the axial direction to optimize the beam profile.

The design of the OASIS ion sources, which deviates in several respects from established practices, will be covered in ref. 18. The main points are as follows:

(1) The electron bombardment ion source operates in a space-charge compensated mode (SC-EBIS) without magnetic field and without support gas per se. This results in high ionization efficiencies (up to 37% for Kr) and a good beam quality. (The total extracted beam current is $\leq 20\ \mu$A.)

(2) All insulators in the hot sections of the ion sources have been eliminated. Instead, electrodes on differing potentials are separated by narrow gaps of typically 0.25 mm width which act as *molecular flow restrictions*. The absense of insulators permits operating temperatures of > 2500°C. The upper temperature limit is determined solely by the vapor pressures of the construction materials (Ta and W).

(3) The coaxial construction of the source assures tight mechanical tolerances even at the highest temperatures, it also provides *active heat shielding*. To illustrate this point: only 650 W of total ion source power (including the filament) are necessary to operate the source near the melting point of Ta (~ 3000°C). The coaxial construction also eliminates cold spots that would act as "cryotraps" for isotopes with high melting points.

(4) In order to introduce low energy recoils – produced in heavy-ion reaction – into the ion source, only very thin windows (~ 1 to 5 mg/cm^2) can be used. The simultaneous requirements for high-temperature operation restrict the choice of the window material to Ta and W. The lifetime of these windows is limited by either evaporation (Ta) or thickening due to the deposition of Ta from the cathode and/or the catcher. Applying again the principle of molecular flow restrictions to this problem makes it possible to eliminate high-temperature windows entirely (fig. 8). The ionizing cavity and the recoil catcher are separated from the target by a bundle of thin-walled Ta capillaries that are maintained at high temperature. Recoils from compound nucleus reactions will traverse this bundle without much attenuation because of their small transverse velocity. Once they have evaporated from the catcher, however, they are prevented by their random motion from diffusing back through the capillaries towards the target. The ratio of the molecular flow conductivities (R) between a large tube (diameter D) and the same tube "filled" with small capillaries is $R > D/d$. This would indicate that the smallest capillaries are the most suitable, but the finite wall thickness and angular spread of the recoils restricts this solution to more realistic values. A suitable compromise is reached when the ratio of the conductivity of the ion source exit opening is significantly larger than the conductivity through the bundle. For the source shown in fig. 8, this can be achieved with about 20 to 30 capillaries.

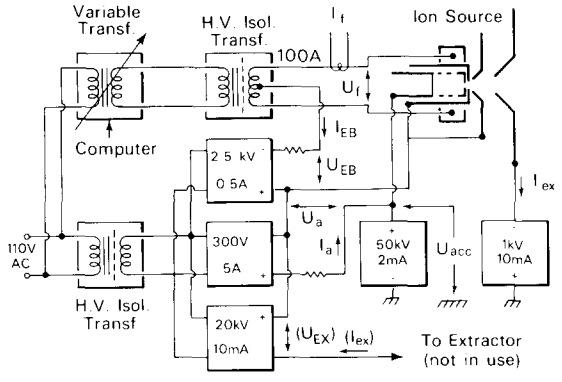

Fig. 9. Power supply connections to the ion source. The abbreviated parameters (I_{ex}, U_{EB}, U_{acc}, etc.) are monitored by the computer, which also controls the variable transformer. (See also fig. 7.)

A simplified block diagram of the electrical connections between the various power supplies and the ion source is shown in fig. 9.

The temperature of the ion source can be measured with an infrared thermometer that "looks" directly into the ion-source opening via a gold-coated mirror. Corrections for the emissivity of various ion source materials are not necessary under these conditions because the geometry is very close to that of a black body radiator.

7. Preliminary off-line and on-line results

The principal goal for an on-line isotope separator is to achieve a modest mass resolution with a good overall efficiency. Although a mass resolution in excess of 2000 can easily be reached with the OASIS magnet, this is of little practical value because it requires narrow entrance and exit slits which reduce the transmission to less than 90%. Under actual running conditions, the entrance "clean-up" slit is about 3 mm wide and the exit slit width is chosen to match the detector parameters and to obtain the required mass resolution. Fig. 10 shows two regions of a mass spectrum obtained under these conditions. These regions were chosen to point out several features of the ion source (SC-EBIS). Under the assumption that the resolution of the spectrometer is predominantly determined by the 2 mm wide exit slit, a theorectical mass resolution of $R_m^{theor} = 590$ can be calculated. The measured value is 580 (fwhm) and the resolution at 10% peak hight is 360, which is adequate for most on-line experiments.

The dominant peaks of the mass spectrum are Ta^+, Ta^{2+}, and CO^+. A comparison between spectra (b) and (c) (fig. 10) shows that the Ta and W ion currents are

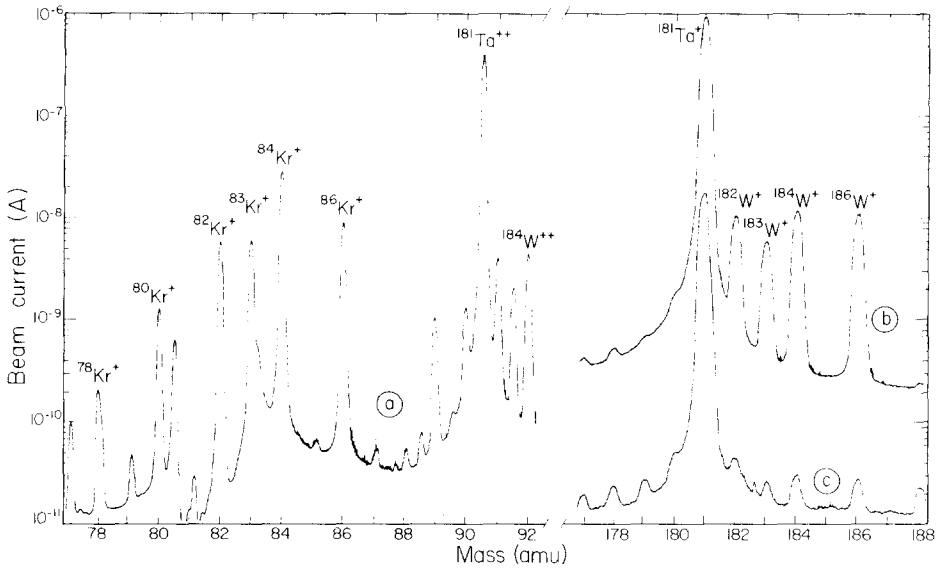

Fig. 10. Mass spectrum of the SC-EBIS ion source in the Kr and Ta regions. Operating parameters are: anode voltage/current: 146 V/0.92 A; total ion source power: 440 W for spectra (a) and (b), and 380 W for spectrum (c); entrance slit: 3.2 mm; exit slit 2 mm; ionization efficiency for Kr $\eta_{Kr} \geq 30\%$; transmission: $\geq 95\%$; electrometer bias current: 10^{-11} A; scan time: 400 s; total output current of the source: 20 μA; Kr leak: 1.37×10^{12} atoms/s.

highly temperature dependent. An increase of only 60 W (16%) in the total ion-source power raises the Ta current by nearly two orders of magnitude. The Ta peaks also show extensive "tailing" due to ions originating in regions of the ion source with potentials different from the main accelerating potential. Such regions are created in several ways, for instance, by the primary electron bombardment electrodes. Fig. 10 also shows the presence of doubly charged ions, which is understandable, considering that the electron energy is 146 V. Almost all peaks in the mass spectrum between 1 and 300 amu can be identified except for several smaller peaks. Highly distorted peaks are often due to higher charge states or molecular ions that decompose during acceleration. Between mass 1 and 300 there exists a "background" peak at every mass number; this is sometimes helpful for mass identification, but, on the other hand, it completely eliminates the possibility of directly counting radioactive ions. The magnitude of these "stable" mass currents is between 10^{-13} and 10^{-10} A.

Several methods have been employed to measure the efficiency of the separator. This efficiency is dominated by that of the ion source, since the ion optical transmission for low mass resolution ($R_m \simeq 500$) is $\geq 95\%$, as pointed out before. In fig. 10, a calibrated Kr leak was connected to the SC-EBIS and the efficiency determined from the known leak rate and the Kr currents. A maximum efficiency for Kr of 36.5% has been obtained. This efficiency can, however, only be achieved at moderate ion source temperatures (< 2400°C); at higher temperatures (~ 2800°C) it decreases to about 30%. The efficiency for Hg is 56%. It was determined from the known vapor pressure of Hg at room temperature. A third method was used for Rn, where the Rn output of a ^{228}Th source was measured via its α-radioactivity and compared to the α-activity in the focal plane of the separator. The efficiency for Rn is 49%.

Preliminary on-line tests of the separator have been carried out with three ion source configurations: surface ionization and electron bombardment ionization for compound nucleus products, and electron bombardment ionization for reaction products of damped collisions. An example of the surface ionization of compound nucleus products is given in fig. 11. A ^{144}Sm target was bombarded with 168 MeV ^{20}Ne ions from the SuperHILAC. The target ion source configuration was similar to that shown in fig. 8. Five masses (152 to 156 amu) were collected simultaneously on the focal plane detectors (fig. 5). Fig. 11 shows the α-spectra of evaporation residue products at different mass positions. The shortest observed half-life is 0.5/0.18 s (^{156}Lu). The efficiency of the surface ionization source in the rare earth region for half-lives of several seconds is about 10%. To test the performance of the surface ion source in the *actinide* region. $^{212/213}$Ac ($T_{1/2} = 0.9/0.8$ s) was produced in a reaction with ^{20}Ne and ^{197}Au. An efficiency of 3 percent was observed. Encouraged by this result, ^{238}U was bombarded with 116 MeV ^{18}O ions and a range of masses collected on a position-sensitive α-detector in the focal plane. In an 8 hour bombard-

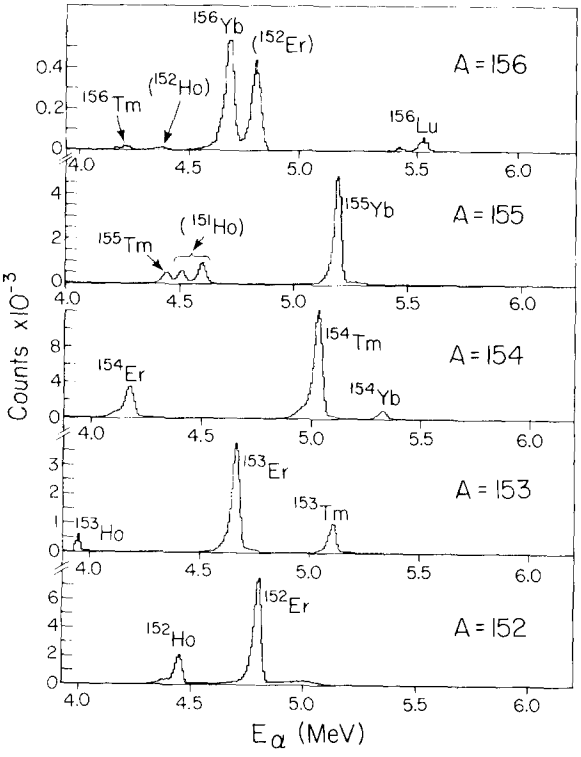

Fig. 11. Alpha spectra obtained with the focal plane detector shown in fig. 5 in the reaction ^{144}Sm (^{20}Ne; xn, yp). The isotopes in parentheses are daughter products.

ment, about 1200 atoms of mass 250 were produced. From the observed α-decay energy (7.42 MeV), it can be concluded that the isotope synthesized in the above reaction was ^{250}Fm. Assuming a cross section of 2 μb [19], the overall efficiency of the separator in the case of ^{250}Fm is calculated to be 10%.

As pointed out in section 6, it is possible to position targets with high melting points close to the ionization region to study isotopes produced in damped collisions. This was tested in the reactions of $^{20/22}$Ne (8.5 MeV/A) on ^{181}Ta in which neutron-rich isotopes of oxygen (^{21}O) and fluorine (^{22}F) were produced. Since the oxygen and fluorine isotopes in this mass range have very similar half-lives, a chemical step was introduced to separate the isobars. The oxygen isotopes were separated as *carbon monoxide* molecules, which are very stable even at the highest temperatures. The decay of these and other neutron-rich β^--emitters was studied with a ΔE–E silicon telescope in the focal plane of the separator. This telescope consisted of a 0.144 mm ΔE and a 10 mm E detector operated at 77 K. Recently, a dual ΔE–E proton telescope was added, and this has allowed us to confirm the discovery of the proton radioactivity of ^{147}Tm [20].

The author wishes to express his gratitude to several coworkers who helped to put this instrument together, in particular L. Archambault who did most of the excellent mechanical work, and L. Stout for his fine designs. Thanks also to A. Wydler for his electronics work, and computer specialist R. Leres. J. Molitoris, W.-D. Zeitz, and M. Cable have worked on recent on-line runs.

References

[1] H.L. Ravn et al., eds., Proc. 10th Int. Conf. on Electromagnetic isotope separators and techniques related to their applications, Nucl. Instr. and Meth. 186 (1981).
[2] J.H. Hamilton et al., eds., Proc. Int. Symp. on Future directions in studies far from stability (1979) (North-Holland, Amsterdam, 1980).
[3] P.G. Hansen, Ann. Rev. Part. Sci. 29 (1979) 69.
[4] H.L. Ravn. Phys. Rep. 54 (1979) 201.
[5] P. Jacquinot and R. Klapisch, Rep. Prog. Phys. 42 (1979) 773.
[6] P.G. Hansen and B. Jonson, Europhys. News 12 (1981) 1.
[7] S. Hoffmann, W. Reisdorf, S. Münzenberg, F.P. Hessberger, J.R.H. Schneider and P. Armbruster, Z. Physik A 305 (1982) 111.
[8] J.M. Nitschke, Nucl. Instr. and Meth. 78 (1970) 45.
[9] J.M. Nitschke, Nucl. Instr. and Meth. 138 (1976) 393.
[10] J.D. Molitoris and J.M. Nitschke, Nucl. Instr. and Meth. 186 (1981) 659.
[11] Karl L. Brown, SLAC Report No. 75, Revision 3 (1972).
[12] D.L. Judd, Rev. Sci. Instr. 21 (1950) 213.
[13] D.L Judd, and R.A. Bludman, Nucl. Instr. 1 (1957) 46.
[14] J. Camplan and R. Meunier, Nucl. Instr. and Meth. 186 (1981) 445.
[15] R. Decker, K.D. Wünsch, H. Wollnick, E. Koglin, G. Siegert and G. Jung, Z. Physik A 294 (1980) 35.
[16] C. Maples and J. Sivak, Lawrence Berkely Laboratory Report No. LBL-9182 (1979).
[17] R. Kirchner, Nucl. Instr. and Meth. 186 (1981) 275.
[18] J.M. Nitschke, to be published.
[19] E.D. Donets, V.A. Shchegolev and V.A. Ermakov, Yadern. Fiz. 2 (1965) 1015.
[20] O. Klepper, T. Batsch, S. Hofmann, R. Kirchner, W. Kurcewicz, W. Reisdorf, E. Roeckl, D. Schardt and G. Nyman, Z. Physik A 305 (1982) 125.